

Surface photometry of WINGS galaxies with GASPHOT

M. D’Onofrio¹, D. Bindoni¹, G. Fasano², D. Bettoni², A. Cava³, J. Fritz⁴, M. Gullieuszik²,
P. Kjærgaard⁵, A. Moretti¹, M. Moles⁶, A. Omizzolo^{7,2}, B.M. Poggianti², T. Valentiniuzzi¹, and J. Varela⁶

¹ Department of Physics and Astronomy, University of Padova, Vicolo Osservatorio 3, 35122 Padova, Italy

² INAF – Padova Astronomical Observatory, Vicolo Osservatorio 5, 35122 Padova, Italy

³ Observatoire de Genève, Université de Genève, 51 Ch. des Maillettes, 1290 Versoix, Switzerland

⁴ Sterrenkundig Observatorium, University of Gent Krijgslaan 281 S9, B-9000 Gent, Belgium

⁵ The Niels Bohr Institute for Astronomy Physics and Geophysics, J. Maries Vej 30, 2100 Copenhagen, Denmark

⁶ Centro de Estudios de Física del Cosmo de Aragon, Plaza San Juan 1, 44001 Teruel, Spain

⁷ Specola Vaticana, 00120 Stato Città del Vaticano

October 13, 2014

ABSTRACT

Aims. We present the B-, V- and K-band surface photometry catalogs obtained running the automatic software GASPHOT on galaxies from the WINGS cluster survey having isophotal area larger than 200 pixels. The catalogs can be downloaded at the Centre de Données Astronomiques de Strasbourg (CDS).

Methods. The luminosity growth curves of stars and galaxies in a given catalog relative to a given cluster image, are obtained all together, slicing the image with a fixed surface brightness step, through several SExtractor runs. Then, using a single Sersic law convolved with a space-varying PSF, GASPHOT performs a simultaneous χ^2 best-fitting of the major- and minor-axis luminosity growth curves of galaxies. We outline the GASPHOT performances and compare our surface photometry with that obtained by SExtractor, GALFIT and GIM2D. This analysis is aimed at providing statistical information about the accuracy generally achieved by the softwares for automatic surface photometry of galaxies.

Results. For each galaxy and for each photometric band the GASPHOT catalogs provide the parameters of the Sersic law best-fitting the luminosity profiles. They are: the sky coordinates of the galaxy center ($R.A.$, $DEC.$), the total magnitude (m), the semi-major axis of the effective isophote (R_e), the Sersic index (n), the axis ratio (b/a) and a flag parameter (Q_{FLAG}) giving a global indication of the fit quality. The WINGS-GASPHOT database includes 41,463 galaxies in the B-band, 42,275 in the V-band, and 71,687 in the K-band. We find that the bright early-type galaxies have larger Sersic indices and effective radii, as well as redder colors in their center. In general the effective radii increase systematically from the K- to the V- and B-band.

Conclusions. The GASPHOT photometry turns out to be in fairly good agreement with the surface photometry obtained by GALFIT and GIM2D, as well as with the aperture photometry provided by SExtractor. In particular, the direct comparison among structural parameters coming from different softwares for common galaxies, indicates that the systematic differences are in general small. The only significant deviations are likely due to the peculiar (and very accurate) image processing adopted by WINGS for large galaxies. The main advantages of GASPHOT with respect to other tools are: (i) the automatic finding of the local PSF; (ii) the short CPU time of execution; (iii) the remarkable stability against the choice of the initial guess parameters. All these characteristics make GASPHOT an ideal tool for blind surface photometry of large galaxy samples in wide-field CCD mosaics.

Key words. Surveys - Galaxies : Clusters : General - Catalogs

1. Introduction

Thanks to the performances of modern CCD detectors and computing systems, several astronomical surveys have had the chance of mapping large sky areas, thus providing the opportunity of measuring photometric and structural properties of thousands of extended sources using relatively short exposure-time imaging. This has been achieved also thanks to automatic surface photometry tools offering robust results and not heavily demanding in terms of computer time. The tools most widely used for the aperture and surface photometry of galaxies are SExtractor (Bertin & Arnouts 1996), GIM2D (Simard 1998), and GALFIT (Peng et al. 2002).

In the framework of the *Wide-field Imaging of Nearby Galaxy-clusters Survey*¹ (WINGS; Fasano et al. 2006), we

have devised the tool GASPHOT (*Galaxy Surface PHOTometry*; Pignatelli et al. 2006), aimed at performing the automatic surface photometry of large galaxy samples. The performances of GASPHOT have been already tested on simulated galaxies and against the results of supervised, single-object photometry by Pignatelli et al. (2006).

In the present paper we present the catalogs obtained running GASPHOT onto the B-, V- and K-band wide-field imaging of the WINGS survey. Moreover, we compare the results of GASPHOT with those obtained by SExtractor, GIM2D and GALFIT. In particular, the comparison with GIM2D has been done using the catalogs obtained running GASPHOT onto the B-band imaging of the MGC survey (Allen et al. 2006) and partly published in Poggianti et al. (2013a).

The paper is organized as follows: in Sec. 2 we recall the features of the WINGS survey in order to set the context in which the GASPHOT database is inserted. Section 3 de-

¹ See the WINGS web-site for all the details of this project at <http://web.oapd.inaf.it/wings>.

scribes the guidelines of the software, the data sample analyzed by GASPHOT, and the typical output files. In Section 4 the GASPHOT photometry is compared with that coming from SExtractor, GIM2D and GALFIT. In Section 5, using the structural parameters coming from GASPHOT, we present the main scaling relations of the WINGS galaxies in the different photometric bands. Our conclusions are drawn in Section 6.

2. The WINGS survey

The WINGS survey (Fasano et al. 2006) is a long term project especially designed to provide a robust characterization of the photometric and spectroscopic properties of galaxies in nearby clusters. The core of the survey is WINGS-OPT (Varela et al. 2009), that is a set of B- and V-band images of a complete, X-ray selected sample of 77 clusters with redshift $0.04 < z < 0.07$. The images have been taken with the Wide Field Camera (WFC, $34' \times 34'$) at the INT-2.5 m telescope in La Palma (Canary Islands, Spain) and with the Wide Field Imager (WFI, $34' \times 33'$) at the MPG/ESO-2.2 m telescope in La Silla (Chile). The optical photometric catalogs have been obtained using SExtractor and are 90% complete at $V \sim 21.7$, which translates to $M_V^* + 6$ at the mean redshift of the survey (Varela et al. 2009). The WINGS-OPT catalogs contain $\sim 400,000$ galaxies in both the V- and B-band. According to Varela et al. (2009, Table D.2), in the whole cluster sample the surface brightness limits at $1.5\sigma_{bkg}$ (σ_{bkg} is the standard deviation per pixel of the background) span the ranges 24.7–26.1 (average value: 25.71) and 25.4–26.9 (average value: 26.39) in the V- and B-band, respectively.

SExtractor catalogs have been obtained also for the near-infrared follow-up of the survey (WINGS-NIR; Valentinuzzi et al. 2009), which consists of J- and K-band imaging of a subsample of 28 clusters of the WINGS-OPT sample, taken with the WFCAM camera at the UKIRT telescope. Each mosaic image covers $\approx 0.79 \text{ deg}^2$. With the SExtractor analysis the 90% detection rate limit for galaxies is reached at $J=20.5$ and $K=19.4$. The WINGS-NIR catalogs contain $\sim 490,000$ and $\sim 260,000$ galaxies in the K- and J-band, respectively. The photometric depth of the WINGS-NIR imaging turned out to be slightly worse than that of the WINGS-OPT imaging. Thus, for the K-band the surface brightness limit at $1.5\sigma_{bkg}$ spans the range 20.6–21.5 (see Table 4 in Valentinuzzi et al. 2009, average value: 21.15).

To give a more complete sketch of the observing material available for WINGS, we just mention that the survey also includes medium-resolution, multi-fiber spectroscopy (WINGS-SPE) and U-band photometry (WINGS-UV) of galaxies in subsamples of the WINGS-OPT cluster sample. We refer to Cava et al. (2009) and Omizzolo et al. (2014) for details about these follow-ups. Finally, it is worth mentioning that we are gathering B-, V- and u'-band OmegaCam@VST imaging (one square degree FOV) of the WINGS clusters in the southern hemisphere (Gullieuszik et al., in preparation).

Besides the aperture photometry catalogs (SExtractor) and the surface photometry catalogs presented here, this huge amount of data has produced morphological catalogs ($\sim 40,000$ galaxies), obtained using the purposely devised automatic tool MORPHOT (Fasano et al. 2012), and spectroscopic catalogs including redshifts (Cava et al. 2009), star formation histories, stellar masses and ages (Fritz et al. 2011), as well as equivalent widths and line-indices (Fritz et al. 2014) of $\sim 6,000$ galaxies.

A complete description of the WINGS database, including the GASPHOT catalogs presented here, can be found in Moretti et al. (2014)

3. The galaxy sample and the GASPHOT catalogs

The surface photometry of galaxies in the WINGS clusters has been performed on the same sample used for the morphological (MORPHOT) analysis, *i.e.* $\sim 40,000$ galaxies with isophotal area larger than 200 pixels at the threshold of $2.5\sigma_{bkg}$. To handle such a large number of galaxies the automatic tool GASPHOT was purposely devised. Details about the software are given in Pignatelli et al. (2006), together with tests of the GASPHOT performances, mainly based on simulated galaxy samples. The code first produces a set of growth curves of stars and galaxies through several runs of SExtractor. Then, for each galaxy, a simultaneous best-fit of the major and minor-axes growth curves is performed using a single 2D Sersic law convolved with a space-varying Point Spread Function (PSF). The fitting strategy of GASPHOT is a sort of hybrid between the 1D equivalent luminosity profile fitting and the 2D full image fitting technique. Pros and cons of these approaches are outlined in Sec. 4.2.6.

The GASPHOT tool is blind, *i.e.* it performs the surface photometry of all galaxies in a given catalog (relative to a given frame) without requiring a first guess of the model parameters for each galaxy, as it occurs for most popular 2D tools. GASPHOT just needs a special care in the choice of the configuration file parameters that mostly influence the observed (PSF convolved) light profiles, in particular the deblending parameter and the detection and analysis threshold parameters of SExtractor (DEBLEND_NTHRESH, DETEC_THRESH and ANALYSIS_THRESH), the surface brightness step and the magnitude range of the stars used to derive the PSF profile (Pignatelli et al. 2006).

After having extracted the major and minor axis growth curves, for each galaxy the best-fitting procedure provides the total magnitude (m), the axis ratio (b/a), the effective radius (R_e), the Sersic index (n), and the χ^2 of the best fit Sersic model. It is worth recalling here that, since the boundary values used by GASPHOT for n are 0.5 and 8, finding these output values of the Sersic index is considered as an indication that the best fitting procedure has been problematic or unsuccessful.

Although GASPHOT considers the background as a free parameter of the best-fitting algorithm, in most cases it is convenient to operate with images in which the background has been already roughly subtracted (for instance with SExtractor) and to refine the subtraction limiting the range of variability of the background parameter in the fitting procedure. Varela et al. (2009) describe in detail the procedure of background subtraction adopted for the WINGS clusters. Here we just recall that the careful modeling and removal of the brightest galaxies and stars (most of them equipped with extended halos) allows to obtain reliable surface photometry parameters of both the bright galaxies themselves and the many small/faint companion galaxies usually embedded inside their halos. Such procedure obviously results also in a very precise determination of the background path to be subtracted from the images. Thus, in our case we have allowed GASPHOT to vary the background parameter of just $1.8 \times \sigma_{bkg}$.

The CPU time needed to run GASPHOT on a sample of ~ 600 galaxies (the typical number of galaxies in WINGS cluster catalogs) is ~ 2 h on a server with a double CPU Xeon E5439 @ 2.6GHz (in total 8 cores) with 16Gb RAM. Most of this time is used by SExtractor to extract the major and minor axis growth curves.

In the paper of Pignatelli et al. (2006) the output parameters of GASPHOT have been compared with results of GIM2D and GALFIT using ~ 15000 simulated galaxies, including multi-component ($r^{1/4} + exp.$) galaxies and blended objects, in a wide

range of magnitude, flattening, and radius. It was found that, for objects with threshold isophotal area greater than 200 pixels, the photometric and structural parameters derived by GASPHOT are in very good agreement with the input values of simulations, even for composite luminosity profiles, blended objects and low surface brightness galaxies. A small number of outliers were found, but the results were robust in a statistical sense. The scatter was in general small ($<15\%$), but for single objects the errors on effective radius R_e and Sersic index n could (in a few cases) exceed 20-40%. Finally, although giving similar results on simulated galaxies, GALFIT and GIM2D were found to be less robust than GASPHOT when using single Sersic model to fit luminosity profiles of real galaxies. The last result relied on a small sample of galaxies having detailed (visually supervised) surface photometry.

The GASPHOT WINGS-OPT sample in the B(V)-band consists of 41, 463 (42, 275) galaxies of all morphological types detected by SExtractor as having isophotal area larger than 200 pixels above $2.5\sigma_{bkg}$. The average number of galaxies per cluster which satisfy the above condition is ~ 560 . Using the same criterion, the GASPHOT WINGS-NIR sample consists of 71, 687 galaxies in the subsample of 28 clusters observed in the K-band (Valentinuzzi et al. 2009) (~ 2750 objects per cluster, on average). The galaxies in common among the B-, V- and K-bands are $\sim 10, 424$ and belong to 25 clusters².

For each galaxy, the GASPHOT catalogs list the WINGS identifier and the best fitting parameters found by GASPHOT for the single Sersic law model. In particular, the coordinates (RA and DEC) of the center, the total magnitude, the effective radius, the Sersic index and the axis ratio (see Table 1). Moreover, for each galaxy, GASPHOT provides the major- and minor-axis grow curves, as well as the ellipticity and position angle profiles of the ellipses best fitting the isophotes. These can be useful to analyze the shape of galaxies, in particular to test the presence of bars.

Not always the quality of the GASPHOT fit can be judged on the basis of the χ^2 parameter, since several effects might influence its value. Among them we mention: the uncertainty on the background value (in particular close to the very bright objects), the choice of the deblending parameters of SExtractor for luminosity profile extraction, the cutting of luminosity profiles for objects close to the CCD borders, the accuracy of the local PSF and, most of all, the presence of galaxy substructures that cannot be represented by the Sersic law, especially when objects are well resolved. On the other hand, the errors provided by GASPHOT for each output parameter turn out to be usually too small, since they are just formal uncertainties associated with the fitting procedure. For these reasons, neither the χ^2 , nor the errors on individual parameters have been included in the catalogs. Instead we preferred to provide possible users with the global quality index Q_{FLAG} . This is a decimal number corresponding to a binary, 8 digits number. The first two digits are always set to 0, while the remaining six are set to 1 when: the Sersic index is equal to 0.5 or 8 (3rd digit), the errors in the estimated parameters (magnitude:4th digit; effective radius:5th digit; Sersic index:6th digit; background:7th digit and axial ratio:8th digit) exceed the 98 percentile of the error distributions for the given image. For instance, $Q_{FLAG} = 0$ for good fits, 32 for fits that have Sersic index equal to 0.5 or 8 (the search interval bound-

Parameter	Units	Description
ID_WINGS	NULL	WINGS object identification
R.A.	[deg]	Central right ascension
DEC.	[deg]	Central declination
m_V	[mag]	Total magnitude
R_e	[arcsec]	Major axis effective radius
n	NULL	Sersic index
b/a	NULL	Axis ratio
Q_{FLAG}	NULL	Quality FLAG

Table 1. The parameters provided by GASPHOT for each galaxy in the V band.

aries used by GASPHOT for the Sersic index), 2 for fits with too large error on the background estimation, 16 for fits with too large error on the estimated magnitude.

The Q_{FLAG} parameter is just an attempt to quantify the problems encountered during the fit of each galaxy. We believe that, rather than for single objects, a reliable estimate of the uncertainties of GASPHOT can be obtained only in a statistical sense. The comparison of GASPHOT with SExtractor, GALFIT and GIM2D can provide us with such statistical uncertainties, thus giving us an idea about the actual limits of the automatic tools for the surface photometry of galaxies (see Sec.4).

The GASPHOT catalogs refer to fairly homogeneous samples in the different bands, since they have been obtained from CCD images whose exposure times have been tuned to reach almost the same photometric depth. Here, we empirically define the photometric depth as the interval $\Delta\mu$ between the brightest and the faintest surface brightness level detected for each galaxy on the CCD image. The above mentioned homogeneity is illustrated in Figure 1, where the $\Delta\mu$ histograms of galaxies in four clusters (two imaged with INT and two with MPG) for the three bands are plotted as an example. Of course, larger values of $\Delta\mu$ correspond to brighter galaxies, but what is noticeable in the figure is that the range of $\Delta\mu$ is almost the same in the three bands ($\sim 4 \div 5$ mag). Therefore, we are confident that, at least as far as the photometric depth is concerned, no statistical biases among the different filters are present in the GASPHOT parameters because of different galaxy sampling.

In Section 2 we recall that, with the typical values of σ_{bkg} found in the WINGS-OPT V-band imaging, we obtain an average value of the isophotal threshold of $\mu_{Thr}(V) \sim 25.7$ mag arcsec⁻². It is worth noticing that, at the same signal to noise level, the images from SDSS in the g- and r-band reach $\mu_{Thr}(g) < 25.2$ mag arcsec⁻² and $\mu_{Thr}(r) < 24.7$ mag arcsec⁻², respectively.

4. Internal and external comparisons

Pignatelli et al. (2006) checked the GASPHOT performances against the results coming from detailed, single-object surface photometry of 231 early type galaxies published by Fasano et al. (2003) and against the surface photometry parameters obtained by Smail et al. (1997) from HST imaging of galaxies in the cluster Abell 370. They found a generally good agreement between automatic (GASPHOT) and single-object surface photometry parameters, although a large scatter and a slight tendency of underestimating the total luminosity and the effective radius of very large galaxies seemed to be present in GASPHOT with respect to the supervised, single-object surface photometry.

In this section we test the GASPHOT results against SExtractor and GALFIT, using the WINGS data, and against GIM2D, using the Padova Millenium Galaxy and Group Catalog

² A119, A500, A602, A957x, A1069, A1291, A1631a, A1644, A1795, A1831, A1983, A2107, A2124, A2149, A2169, A2382, A2399, A2457, A2572a, A2589, IIZW108, MKW3s, RX1022, RX1740, Z8338.

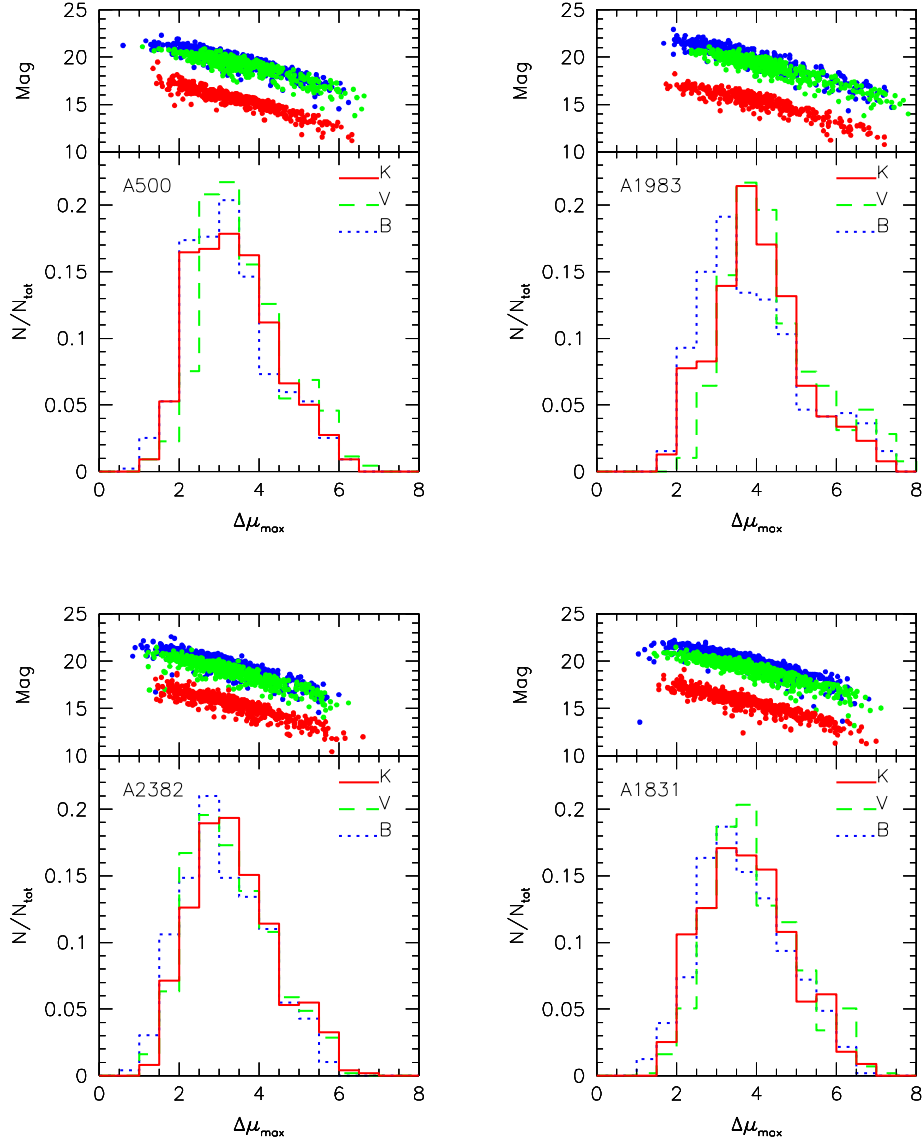


Fig. 1. Histograms of the photometric depth $\Delta\mu_{\max}$ observed in the B, V and K bands for four different WINGS clusters (A500, A1983, A2382 and A1831). The color legend marks the various filters. The upper panels above each histogram show the total luminosity versus $\Delta\mu_{\max}$.

PM2GC (Calvi et al. 2011). In each comparison we use only galaxies with *SExtractor* flag equal to zero and found by *SExtractor* as having threshold area (above $2.5\sigma_{bkg}$) greater than 200 pixels. Moreover, we decided to exclude from this comparison those galaxies for which GASPHOT gives $n=0.5$ or $n=8$ (boundary values for the search n interval), as well as those for which, according to GASPHOT, the average surface brightness within the effective isophote turns out to exceed 21.5, 25.5 and 26.5 for the K-, V- and B-band, respectively. In fact, according to the quality index Q_{FLAG} , beyond these values the surface photometry parameters provided by GASPHOT for our galaxy samples becomes largely unreliable.

4.1. GASPHOT vs. *SExtractor*

In Figure 2 the median total magnitude differences Δm between *SExtractor* and GASPHOT in the K-, V- and B-band (top to bottom) are binned as a function of the best fit quantities derived by GASPHOT. They are (left to right): the absolute magnitude, the effective radius and surface brightness, the Sersic index and the axis ratio. The error bars represent the *r.m.s* uncertainty of the median values in each bin. The number of galaxies used for the comparisons are 7485, 23378 and 22309 for the K-, V- and B-band, respectively.

The most evident feature in Figure 2 is the dependence of Δm on galaxy size in all wavebands. For large galaxies, the *SExtractor* magnitudes turn out to be fainter than the GASPHOT ones. We have verified such a trend to be particularly evident for late-type galaxies in the B-band. This depends on the fact that, in spite of the accuracy in choosing the de-

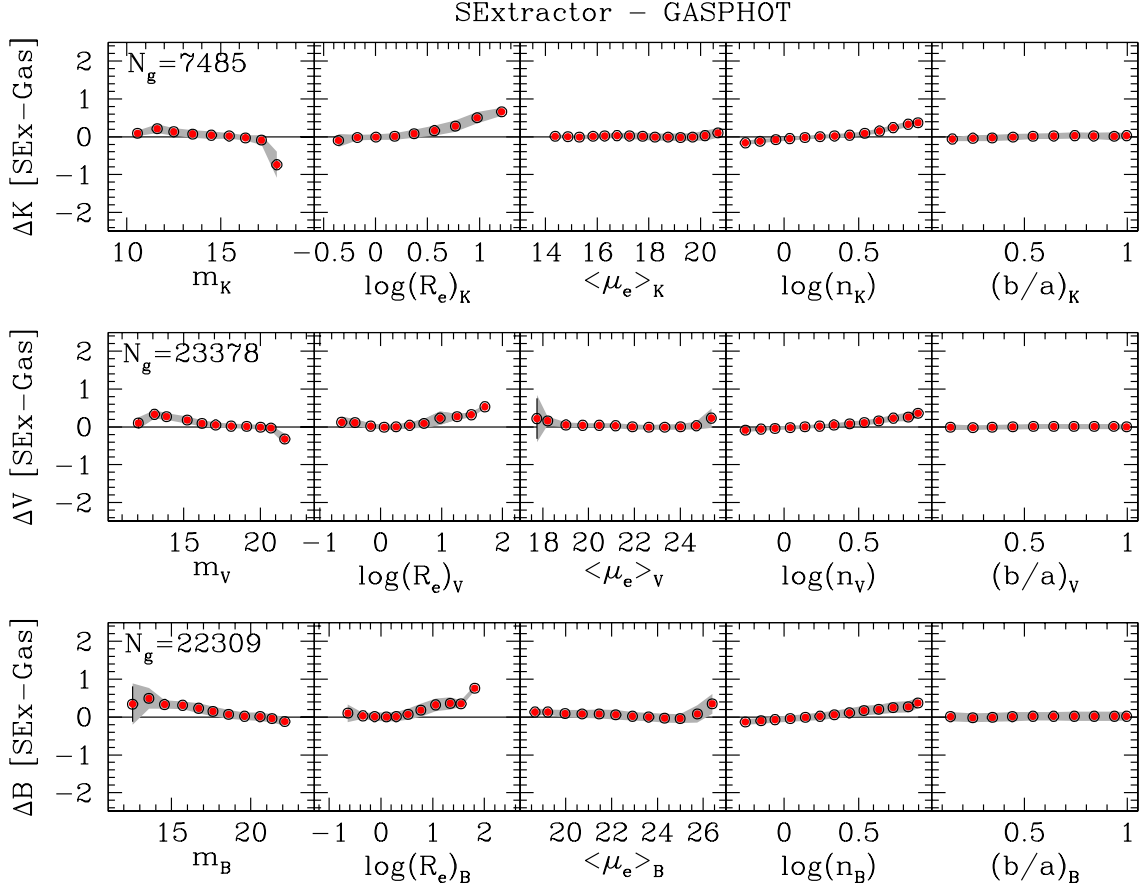


Fig. 2. Median total magnitude differences between SExtractor and GASPHOT in the K-, V- and B-band (top to bottom) binned as a function of the absolute magnitude, the effective radius and surface brightness, the Sersic index and the axis ratio derived by GASPHOT (left to right). The error bars represent the uncertainties of the median values in each bin, while the shaded bands give the semi-inter quartile ranges of the distributions of the deviations. In this case, both quantities are very small (comparable with the size of the points). The sizes of the samples used for the comparisons are reported in the leftmost panel for each filter

blending parameters, in many cases SExtractor tends to erroneously split large spirals into multiple, smaller objects (HII regions and other light blobs). Instead, in the case of early-type galaxies, the magnitude difference, still present and positive, reflects the well known inability of SExtractor to extrapolate the smoothly decreasing (high Sersic index) outer profiles of galaxies (Franceschini et al. 1998). This is confirmed by the smooth rise of Δm as a function of the Sersic index in all wavebands (see Figure 2), as well as by the attenuation of the bias when the first three ranked most luminous galaxies in each cluster are removed from the WINGS sample. The dependence of Δm on galaxy size also determines the behavior of Δm as a function of the luminosity. Instead, no dependence at all of Δm on the axial ratio is found.

4.2. GASPHOT vs. GALFIT and GIM2D

Pignatelli et al. (2006) showed that the performances of GASPHOT on artificial galaxies are similar to those of GALFIT and GIM2D for large and regular galaxies, while for automatic surface photometry of small galaxies and blended objects, GASPHOT provides more robust results than GALFIT and

GIM2D (see Cols. 6 and 9 of Table 1 and Figs. 12 and 13 in Pignatelli et al. (2006)). This is a crucial feature when dealing with blind surface photometry of huge galaxy samples.

In this section, we use real galaxies to perform the comparison between the automatic surface photometry parameters from GASPHOT and from the above mentioned tools GALFIT and GIM2D. For both comparisons (GALFIT-GASPHOT and GASPHOT-GIM2D) the model used to fit the galaxy luminosity profiles was the single 2D Sersic law, with constant ellipticity and position angle.

4.2.1. Samples used for the comparisons

For the comparison between GASPHOT and GALFIT, we use a sample of 1684 galaxies randomly extracted from the WINGS-GASPHOT catalogs among those having $Q_{FLAG} = 0$ and belonging to clusters whose V-band WINGS-OPT imaging has been obtained in good seeing conditions, with minimal PSF variation over the cluster field. On this galaxy sample GALFIT has been run taking as initial guess for the parameters the V-band photometric and geometric quantities provided by the WINGS-OPT SExtractor catalogs.

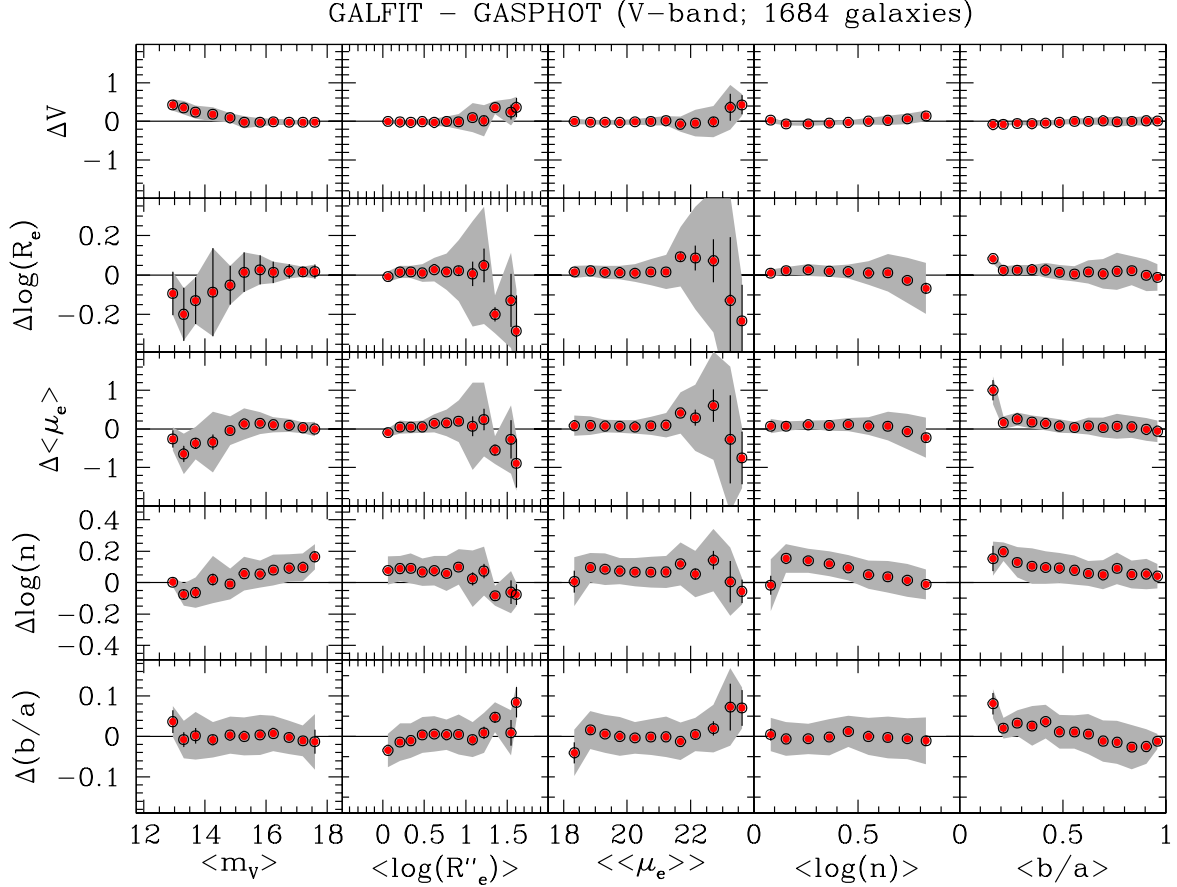


Fig. 3. Comparison between the results of GASPHOT and GALFIT surface photometry for 1684 galaxies randomly extracted from the WINGS V-band catalogs. The comparison is made for apparent total magnitude, effective radius in arcseconds, effective average surface brightness, Sersic index and axis ratio. The above parameters in abscissa are averaged between the tools under comparison, while the differences between the values found by the tools are reported for each parameter on the ordinate, binned over the whole set of parameters. As in Fig. 2, the error bars represent the uncertainties of the median values of the differences in each bin, while the shaded bands give the semi-inter quartile ranges of the distributions of the deviations.

The CPU time required by GALFIT to produce the surface photometry parameters of a single galaxy turned out to be (on average) about 2 times longer than in the case of GASPHOT. This is likely because GALFIT has to handle the whole set of pixels belonging to each galaxy, while GASPHOT just deals with the major and minor axis growth curves.

The comparison between GIM2D and GASPHOT has been performed using galaxies in a sub-sample of the Millennium Galaxy Catalog (hereafter MGC; Liske et al. 2003; Cross et al. 2004). The MGC survey is based on B band imaging taken with the WFC camera of the Isaac Newton Telescope (the same used by WINGS in the northern hemisphere; pixel size of 0.333 arcsec) along an equatorial strip covering an area of $\sim 37.5 \text{ deg}^2$. The MGC images reach an isophotal detection limit of $26.0 \text{ mag arcsec}^{-2}$.

The GIM2D data come from three different works based on the MGC imaging: the surface photometry by Allen et al. (2006), that of the New York University Value Added Catalogue (NYUVAC Blanton et al. 2005), and that from the SLOAN DR7 data (Simard et al. 2011).

We have obtained GASPHOT surface photometry for a sample of galaxies in the PM2GC (Calvi et al. 2011), that is a galaxy

catalog extracted from the MGC and representative of the general field population in the local Universe ($0.04 \leq z \leq 0.1$).

A preliminary comparison between GASPHOT and GIM2D was presented by Poggianti et al. (2013a) for 618 galaxies in common between the PM2GC and MGC surveys. Poggianti et al. (2013a) found that the agreement between GASPHOT and GIM2D is generally good, with a tendency for the GASPHOT radii to be slightly larger than the others. The median difference between the effective radii R_e is about $0.03 \pm 0.04 \text{ dex}$ with respect to the data of Allen et al. (2006), $0.03 \pm 0.06 \text{ dex}$ with respect to the NYUVAC, and $-0.01 \pm 0.04 \text{ dex}$ with respect to Simard et al. (2011).

In the present paper, the comparison between GASPHOT and GIM2D has been done using an extended sample of 2581 galaxies in common between the PM2GC and MGC surveys.

Since for this comparison we use GIM2D literature data, in this case we are not allowed to directly compare the average CPU time required by the tools to produce the surface photometry parameters of a single galaxy. However, it is worth recalling that GIM2D was found by Pignatelli et al. (2006) to be significantly more expensive in terms of CPU time with respect to both GASPHOT and GALFIT.

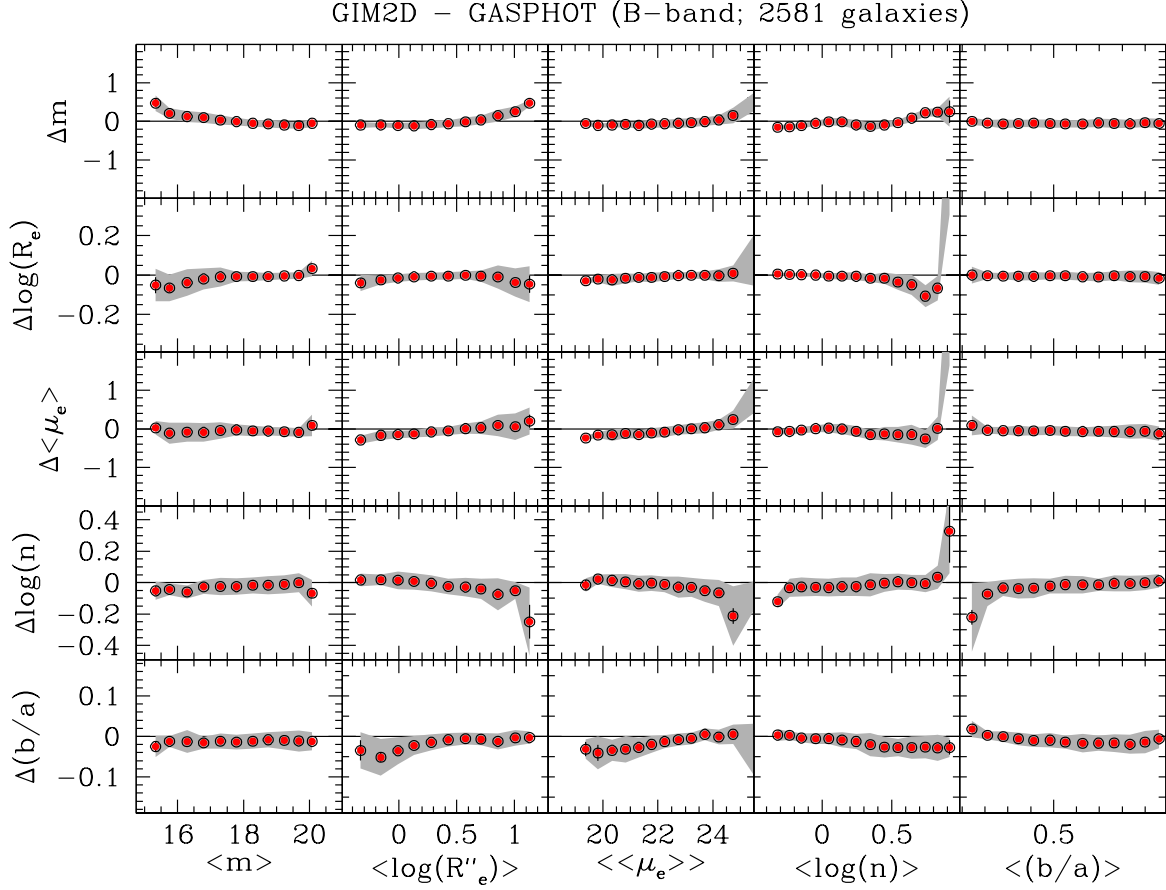


Fig. 4. Same as Fig. 3, but for the GIM2D - GASPHOT comparison (B-band) on the sample of 2581 galaxies in common between the surveys PM2GC and MGC (Allen et al. 2006).

To discuss in detail the features of GASPHOT, GALFIT and GIM2D is beyond the scope of this paper. The reader can find them in the above cited papers. Neither we aim here to propose a ranking of goodness for the three tools. The comparison we are going to perform in this section is just intended at providing an estimate of the uncertainties of the surface photometry parameters obtained with automatic tools. Still, it can be useful to summarize here how the data used for the comparison have been obtained, in particular in the matter of the sky background subtraction, the PSF modeling and the best-fitting scheme.

4.2.2. Sky subtraction

The WINGS images used here for both GASPHOT and GALFIT surface photometry have already been sky subtracted using the procedure described in Varela et al. (2009, see also Section 2).

GASPHOT can use the sky level I_{bkg} as a free model-parameter of the best-fitting procedure. However, since this could be dangerous, particularly for blended objects, the user can limit the range of variation for this parameter when one is confident that a careful sky subtraction has already been performed on the images. This is our case and we allowed I_{bkg} to vary of $1.8 \times \sigma_{bkg}$ at most.

GALFIT can also consider the sky level I_{bkg} as a free model-parameter of the best-fitting procedure. However, since no re-

stricted range of I_{bkg} variation is allowed in GALFIT, we preferred not to include it among the free parameters, fixing its value at zero.

The treatment of the background subtraction is not homogeneous in the literature sources of the GIM2D surface photometry data used for the present comparison (Blanton et al. 2005; Allen et al. 2006; Simard et al. 2011). It ranges from a crude SExtractor estimate of the global sky level to a more accurate determination, adopting for each galaxy a minimum distance of background pixels from object pixels, defined by segmentation mask images.

4.2.3. PSF modeling

GASPHOT automatically extracts the profiles of the stars, models the variation of the FWHM through the field with a 2D polynomial of user-defined degree, and combines the PSF profiles, after having re-scaled them according to the space varying model obtained previously. Finally, a multi-Gaussian function is used to perform the χ^2 best-fitting of the average PSF profile. The Sersic profiles are then convolved with a PSF whose gaussian coefficients depend on the position of the galaxy in the frame.

Both GALFIT and GIM2D assume the user to be able to provide for each galaxy a suitable PSF, both from star images or by functional form. When running GALFIT on our sample

of WINGS galaxies, we decided to adopt a single average PSF image for each cluster, so we could not account for minor PSF differences over the image. However, due to the previously outlined choice of the WINGS imaging for the GASPHOT-GALFIT comparison, this should not significantly contribute to worsen the results.

Again, in the case of GIM2D the determination of the PSF is not homogeneous in the literature data used for the present comparison, ranging from a unique PSF for all galaxies in a given image to a more sophisticated (space varying) treatment, as well as from a simple gaussian profile to a more complex (functional or user-defined) form.

4.2.4. Best-fitting

GALFIT uses the Levenberg-Marquardt downhill-gradient method to derive the best fit. An error map image is automatically produced by the software. At each pixel position the Poisson error is evaluated on the basis of the gain and read-noise parameters contained in the image header. Good fits can be obtained only when the error map is well known and used as weighting image.

The Metropolis best fitting algorithm used by GIM2D (Metropolis et al. 1953; Saha & Williams 1994) is more CPU expensive than the Levenberg-Marquardt downhill-gradient method used by GALFIT. However, it is claimed to be particularly suited to explore a n-dimensional parameter space (with n possibly larger than 10) having a very complicated topology with local minima at low S/N ratios. As in GALFIT, a noise map is used to weight pixels.

After having produced the isophotes of all galaxies together (see Section Sec2), GASPHOT performs, for each galaxy, a simultaneous Levenberg-Marquardt χ^2 best-fit of the major and minor axis growth curves with a 2D Sersic law, convolved with the proper PSF. Each point of the growth curves is weighted according to the statistical uncertainties on both the integrated isophotal magnitude and the radius (pixellation). With respect to the S/N driven, pixel-by-pixel weighting, commonly used in the genuine 2D tools, this procedure tends to overweight the outer part of the profiles, being less sensitive to the high- S/N peculiar features (dust-lanes, cores, small bars and rings, etc...) often affecting the innermost galaxy body. This is likely to make GASPHOT particularly useful when dealing with large/huge galaxy samples, for which detailed, single-object (visually supervised) modeling must be sacrificed to the advantage of speed and robustness.

4.2.5. Results

Figures 3 and 4 illustrate the differences between surface photometry parameters for the GALFIT-GASPHOT and GIM2D-GASPHOT comparisons, respectively. The surface photometry parameters used for the comparisons are: the apparent total magnitude, the effective radius in arcseconds, the effective average surface brightness, the Sersic index and the axis ratio. Since we cannot a priori assume one of the tools to give more reliable results than the others, in both figures, the above parameters in abscissa are averaged between the tools under comparison. The differences between the values found by the tools are reported for each parameter on the ordinate, binned over the whole set of parameters. Moreover, the error bars in the figures represent the 1σ uncertainties of the median values of the differences in each

GALFIT-GASPHOT					
	Δm	$\Delta \log R_e$	$\Delta \langle \mu \rangle_e$	$\Delta \log n$	$\Delta (b/a)$
$\langle \Delta \rangle$	-0.020	0.016	0.086	0.077	-0.001
σ_Δ	0.123	0.077	0.320	0.116	0.067
GIM2D-GASPHOT					
$\langle \Delta \rangle$	-0.068	-0.006	-0.049	-0.014	-0.012
σ_Δ	0.125	0.030	0.187	0.080	0.028

Table 2. Global median values and *r.m.s.* of the differences (GALFIT-GASPHOT) and (GIM2D-GASPHOT) are reported for the apparent magnitude (V- and B-band, for the first and second comparison, respectively), the effective radius and surface brightness, the Sersic index and the axis ratio.

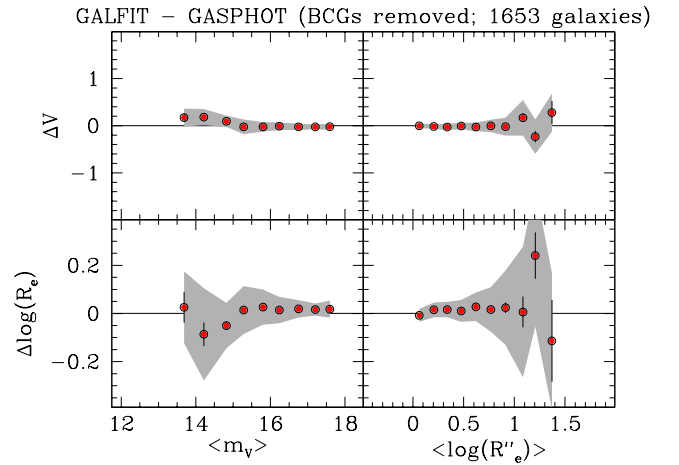


Fig. 5. Apparent magnitude and effective radius comparison between GASPHOT and GALFIT for the sample of Fig. 3, after removal of the BCGs. In this case the size-driven bias visible in Fig. 3 turns out to be much lower or even absent (see text).

bin, while the shaded bands give the semi-inter quartile ranges of the distributions of the deviations.

In Table 2 the global median values and *r.m.s.* of the differences (GALFIT-GASPHOT) and (GIM2D-GASPHOT) are reported for the same surface photometry parameters used in Figs. 3 and 4.

From these figures and from Table 2 first we note that the general agreement is better and the scatter smaller for the GIM2D-GASPHOT than for the GALFIT-GASPHOT differences. This cannot be due to the different size of the two samples (2581 vs. 1684), since a larger scatter in the GALFIT-GASPHOT plots is found even considering just early-type galaxies (plot not shown), for which the sample size is greater for the GALFIT-GASPHOT than for the GIM2D-GASPHOT comparison (1491 vs. 1126). Thus, either we should guess the intrinsic uncertainty to be larger for GALFIT than for GIM2D or, alternatively, we could speculate about a sort of environment driven, additional scatter, making the surface photometry of galaxies less reliable in the cluster (GALFIT) than in the general field (GIM2D) environment.

A second thing worth noting in the plots is the dependence of the scaling quantities differences (Δm , $\Delta \log(R_e)$ and $\Delta \langle \mu \rangle_e$) on the galaxy scaling parameters themselves. In particular, for large and bright galaxies, GASPHOT seems to produce best-fit galaxy models brighter and larger than GALFIT and (just marginally!) GIM2D. Since the same happens for the SExtractor-GASPHOT comparison (see Fig. 2), we could be induced to conclude this behaviour to be due to some size-driven bias of the GASPHOT surface photometry (although an opposite tendency has been noted before; see the first sentence of Sec. 4). However, we ruled out this conclusion on the basis of the following arguments:

(i) the above mentioned inability of SExtractor to extrapolate the smoothly decreasing (high Sérsic index) outer profiles of bright galaxies is likely responsible of the size-driven magnitude differences between SExtractor and GASPHOT, particularly for less deep imaging, as in the case of the B- and (even more) K-band WINGS imaging;

(ii) the agreement with the GIM2D photometry looks quite better than for the other comparisons. In particular, the size-driven differences are much less evident and some of the systematic differences present in the GALFIT-GASPHOT comparison disappear, or even behave in the opposite direction (see for instance $\Delta \log(n)$ and $\Delta \langle \mu \rangle_e$);

(iii) a natural attitude of GASPHOT to well represent the outer luminosity profiles of large (halo-equipped) galaxies should be expected, because of the GASPHOT tendency of over-weighting the outer regions of galaxies with respect to the other tools (see Section 4.2.4). We think the most evident size-driven differences between GALFIT and GASPHOT to be actually due to this different weight allocation, which is particularly effective for large, luminous galaxies. To this concern, it is interesting to note that these systematic differences almost disappear if we exclude from the sample the BCGs (Figure 5).

4.2.6. Final remarks

In general, the presence of systematic differences among the parameters provided by different surface photometry tools should not amaze anybody, since they are naturally expected because of the different surface photometry techniques adopted by the tools. As mentioned in Section 3, the GASPHOT algorithm is a sort of hybrid between the 1D (equivalent luminosity profile fitting) and 2D (full image fitting) approach.

Of course, pros and cons can be found for both approaches. As a general rule, even if the 1D technique is unable to model either the inner (seeing-affected) regions of flattened galaxies or possible misalignments between different galaxy components, it has the advantage of being less sensitive to the peculiar features of real galaxies, since the elliptical isophotes are averaged over a large number of pixels and their parameters (coordinates of the center, semi-major axis, ellipticity and position angle) can be derived even for very noisy and irregular shapes. On the contrary, the 2D approach is fully equipped to handle the above mentioned issues (convolution of seeing-affected regions of flattened galaxies and modeling of misalignment between different galaxy components), but its sensitivity to the galaxy peculiar features makes dangerous its blind (not supervised) application to large galaxy samples, since it might produce unrealistic results for a fraction of the sample. Roughly speaking, the 1D approach is more robust, since it provides reasonable results even in critical situations, while the 2D approach is suitable for supervised, detailed modeling of well-sampled objects, even for multi-component structures and in the very inner region of galaxies (Haussler et al.

2007; Pignatelli et al. 2006; Lotz et al. 2006; Blanton et al. 2003; Bershadsky et al. 2000).

GASPHOT tries to exploit the robustness of the 1D fitting technique, keeping at the same time the capability of dealing with PSF convolution in the innermost regions typical of the 2D approach. GASPHOT substantially reduces the amount of interaction for the user and (mainly working in blind mode) is able to provide robust estimates of the relevant global parameters for the hundreds of galaxies typically found in wide/deep-field images.

4.3. GASPHOT parameters in different bands

After having checked the results of GASPHOT against the alternative tools GALFIT and GIM2D, in this section we compare among each other the structural parameters obtained by GASPHOT in the B-, V- and K-band.

In Figure 6 the various structural parameters obtained by GASPHOT in the different bands are compared as a function of the parameters themselves, averaged between the filters under comparison. In particular, the upper panels refer to the B- vs. V-band comparison, while the lower panels illustrate the V- vs. K-band comparison. In the plots comparing the total magnitude and the effective surface brightness, in order to emphasize the trends of the relations, the Δm and $\Delta \langle \mu \rangle_e$ differences are ‘normalized’ by subtraction of the average colors, *i.e.* the total magnitude differences, averaged over the whole samples.

For all the photometric and structural parameters, the agreement between the B- and V-band turns out to be fairly good. Moreover, no significant trends are found, apart from a slight tendency of faint, small galaxies and a more marked tendency of high Sérsic index galaxies to be redder. Instead, in the plots comparing the V- and K-band GASPHOT parameters, the general agreement looks a bit worse with respect to the previous case. In addition, various offsets and trends are visible at a glance. In particular, compared with the V-band, the structure of galaxies in the K-band shows (on average) larger Sérsic index, smaller effective radius and brighter effective surface brightness, even after removal of the global galaxy color. In addition, the tendency (already mentioned for the B- vs. V-band comparison) of high Sérsic index galaxies to be redder becomes much more evident in the V- vs. K-band. All these facts are consistent with the picture proposed by D’Onofrio et al. (2011, see also D’Onofrio et al. 2013b), in which, at increasing the stellar mass (luminosity), early-type galaxies become on average ‘older’ (redder) and more centrally concentrated (higher Sérsic index). The dependence of the effective radius on the waveband has been also discussed in Poggianti et al. (2013a).

5. V-band structural parameters of galaxies in the WINGS clusters

In this Section we briefly illustrate a few statistical properties of the structural parameters of WINGS galaxies and some relations among them. In order to produce the plots presented in this Section, the galaxy sample described in Sec. 4 has been further restricted to include just the spectroscopic members of WINGS clusters for which we have V-band GASPHOT surface photometry (3,131 galaxies). Relying on the morphological classification obtained by MORPHOT, we divided this sample in four, broad morphological types: (i) elliptical galaxies ($T=-5$, 952 objects); (ii) S0 galaxies ($-5 < T \leq 0$, 1478 objects); (iii) early spirals ($0 < T < 5$, 593 objects); (iv) late spirals ($T \geq 5$, 108 objects).

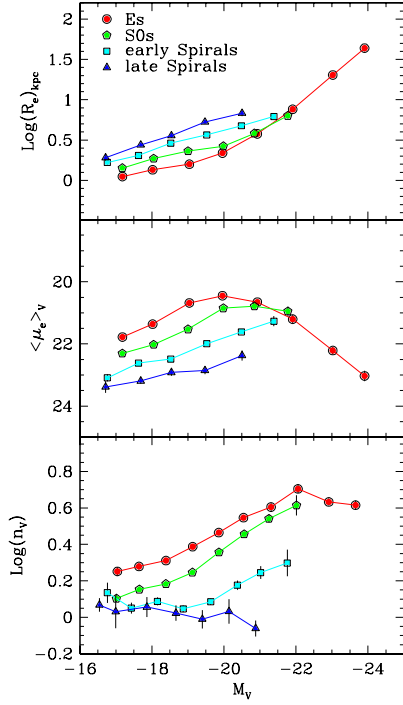


Fig. 7. Effective radius (upper panel), mean surface brightness and Sersic index (lower panel) obtained by GASPHOT for the WINGS galaxies in the V-band as a function of the absolute magnitude for the four, broad morphological types. The mean values of the structural parameters are binned over the absolute magnitude. Ellipticals, S0s, early and late spirals are respectively represented by circles, pentagons, squares and triangles (red, green, cyan and blue in the electronic version).

Figure 7 illustrates how the structural parameters obtained by GASPHOT for the WINGS galaxies in the V-band, depend on the absolute magnitude for the four, broad morphological types. It shows that, for a given absolute magnitude, the later the morphological type, the lower the Sersic index and the larger the effective radius and surface brightness. Moreover, at increasing the total luminosity, the effective surface brightness decreases (with the notable exception of the brightest Ellipticals), while both the Sersic index and the effective radius increase, with the exception of the Sersic index of late spirals, which slightly decreases at increasing the total luminosity. Similar trends have been found in the recent literature (Cebrián & Trujillo 2014; Bernardi et al. 2014).

Note that the brightest Ellipticals show a strong overturning of the surface brightness trend and a less pronounced (but still clear) break of the Sersic index trend. The last feature, not present in the classical relation discovered by Caon et al. (1993) for the Virgo cluster galaxies, has likely emerged here because of the much more robust statistics on the BCGs. These features, together with the marked increase of their size at increasing the total luminosity, are consistent with the picture of BCGs as a separate class of objects, distinct from normal Ellipticals and dominated by the cD galaxies (Capaccioli et al. 1992; Fasano et al. 2010).

In Figure 8 the distributions of the same structural parameters of Fig. 7 (besides the ellipticity), normalized to the area subtended by the histograms, are reported for the four, broad morphological types. It is worth noting the remarkable continuity of the distributions when moving from Elliptical galaxies towards later types. To this concern, the ellipticity distributions constitute, in some sense, an exception, since the flattening distribution of Es looks quite different from those of any other morphological type, in agreement with previous analyses (Fasano & Vio 1991; Fasano et al. 1993, 2010).

Finally, in Figure 9 we plot onto the plane $\langle\mu\rangle_e - \log(R_e)$ the galaxies of the four, broad morphological types, in turn divided in two subsamples, according to the Sersic index (full dots: $n>3$; crosses: $n\leq 3$). The well known Kormendy relation (KR; Kormendy 1977; Capaccioli et al. 1992) seems to hold just for high Sersic index Elliptical galaxies. It looks much less evident (and with a different slope) for low Sersic index Es and S0s, while it is not present at all for spiral galaxies, at least when a single Sersic law is used to represent their luminosity profiles. The large scatter of the KR even for Es with $n>3$ turns out to be reduced if we consider just galaxies with isophotal area larger than 10^3 pixels at $2.5\sigma_{\text{bkg}}$ (full dots in Figure 9).

6. Conclusions

In this paper we have presented the B-, V- and K-band structural parameters of the WINGS cluster galaxies with isophotal area larger than 200 pixels at the threshold of $2.5\sigma_{\text{bkg}}$ in each band. The surface photometry has been obtained by means of the automatic tool GASPHOT, which performs a simultaneous χ^2 best-fitting of the major- and minor-axis growth curves of galaxies using a single Sersic law convolved with a space-varying PSF. For each cluster of the WINGS survey, GASPHOT produced catalogs for the three photometric bands. The catalogs, available at the CDS, provide, for each galaxy, the WINGS identification, the coordinates of the galaxy center, the total magnitude, the effective radius, the Sersic index, the axis ratios and a quality index flag related to the goodness of each fit.

Thank to the database presented here, several thousands galaxies in nearby clusters have now a robust characterization of their structural properties. These data have been already used in many papers of the WINGS series (see e.g., D’Onofrio et al. 2013b; Poggianti et al. 2013c,b; D’Onofrio et al. 2013a; Poggianti et al. 2013a; Vulcani et al. 2012; Fasano et al. 2012; Vulcani et al. 2011b,a; Bettoni et al. 2011; D’Onofrio et al. 2011; Ascaso et al. 2011; Valentinuzzi et al. 2010b; Fasano et al. 2010; Valentinuzzi et al. 2010a; Poggianti et al. 2009). The WINGS database, including the GASPHOT catalogs, is useful for comparing the results of high redshift surveys with the zero point reference frame of objects at low redshifts. A complete description of this database can be found in Moretti et al. (2014).

The GASPHOT output has been tested through direct comparisons against SExtractor (just for total magnitudes), GALFIT and GIM2D. The comparison with GALFIT has been done in the V band using a subset of the WINGS data, while that with GIM2D made use of the PM2GC data in the B band. The agreement among GASPHOT and the above mentioned photometric tools turned out to be generally good, apart from the tendency of SExtractor to progressively underestimate the luminosity of large/bright galaxies with respect to GASPHOT (see Sec. 4.1). A similar (less pronounced), size-driven bias seems to be present also when comparing the total magnitudes from GASPHOT with those coming from GALFIT. However, such a bias disappears if we remove the BCGs from the comparison

sample. This is likely due to the GASPHOT tendency of over-weighting the outer regions of galaxies with respect to the other tools, this tendency being particularly effective for large, luminous galaxies (see Sec. 4.2.4).

The uncertainties of the surface photometry parameters can be estimated looking at the scatter of the differences among the values of the parameters obtained using different tools. In particular, the average uncertainty of the total luminosity is $\sim 12\%$ for both the GALFIT-GASPHOT and GIM2D-GASPHOT differences. Instead, the average uncertainties of the other surface photometry parameters turn out to be significantly lower for the GIM2D-GASPHOT than for the GALFIT-GASPHOT differences. They range from 7% to 20% for the effective radius and from 20% to 30% for both the effective surface brightness and the Sersic index. These uncertainties are likely due to various effects, as already discussed by Pignatelli et al. (2006) and Haussler et al. (2007). Among them we stress the intrinsically different “philosophy” of the 1D approach followed by GASPHOT with respect to the 2D approach followed by GALFIT and GIM2D. We have seen that these two methods have a different sensitivity to the peculiar features of galaxies and behave differently in weighting the various (inner/outer) galaxy regions.

The comparison among GASPHOT results in different wavebands shows a fairly good agreement. Moreover, the trends observed in the colors (especially the V-K) as a function of $\langle\mu\rangle_e$ and of the Sersic index, are consistent with the picture proposed by D’Onofrio et al. (2011, see also D’Onofrio et al. 2013b), in which, at increasing the stellar mass (luminosity), early-type galaxies become on average ‘older’ (redder) and more centrally concentrated (higher Sersic index).

In conclusion, GASPHOT has proven to be effective in performing automatic, blind surface photometry of galaxies in the intermediate and low spatial resolution regime (ground-based, wide-field imaging at low redshift or space-based imaging at intermediate redshift). In these cases, GASPHOT is able to quickly provide robust structural parameters of large galaxy samples. We plan to use GASPHOT to obtain the surface photometry of galaxies in the wide-field images of many southern clusters taken with OmegaCam@VST in the framework of the WINGS survey.

Acknowledgements. The thank Ignacio Trujillo for his help in the analysis of the WINGS galaxies with GALFIT.

References

Allen, P., Driver, S., Graham, A., et al. 2006, *MNRAS*, 371, 2
 Ascaso, B., Aguerri, J. A. L., Varela, J., et al. 2011, *ApJ*, 726, 69
 Bernardi, M., Meert, A., Vikram, V., et al. 2014, *MNRAS*, 443, 874
 Bershad, M. A., Jangren, A., & Conselice, C. J. 2000, *AJ*, 119, 2645
 Bertin, E. & Arnouts, S. 1996, *A&AS*, 177, 393
 Bettoni, D., Kjærgaard, P., Milvang-Jensen, B., et al. 2011, *Astronomische Nachrichten*, 332, 299
 Blanton, M., Schlegel, D., Strauss, M., et al. 2005, *AJ*, 129, 2562
 Blanton, M. R., Hogg, D. W., Bahcall, N. A., et al. 2003, *ApJ*, 592, 819
 Calvi, R., Poggianti, B., & Vulcani, B. 2011, *MNRAS*, 416, 727
 Caon, N., Capaccioli, M., & D’Onofrio, M. 1993, *MNRAS*, 265, 1013
 Capaccioli, M., Caon, N., & D’Onofrio, M. 1992, *MNRAS*, 259, 323
 Cava, A., Bettoni, D., Poggianti, B. M., et al. 2009, *A&A*, 495, 707
 Cebrián, M. & Trujillo, I. 2014, *MNRAS*, 444, 682
 Cross, N., Driver, S., Liske, J., et al. 2004, *MNRAS*, 349, 576
 D’Onofrio, M., Bettoni, D., Bindoni, D., et al. 2013a, *Astronomische Nachrichten*, 334, 373
 D’Onofrio, M., Fasano, G., Moretti, A., et al. 2013b, *MNRAS*, 435, 45
 D’Onofrio, M., Valentinuzzi, T., Fasano, G., et al. 2011, *ApJ*, 727, L6
 Fasano, G., Amico, P., Bertola, F., Vio, R., & Zeilinger, W. W. 1993, *MNRAS*, 262, 109

Fasano, G., Bettoni, D., Ascaso, B., et al. 2010, *MNRAS*, 404, 1490
 Fasano, G., Marmo, C., Varela, J., et al. 2006, *A&A*, 445, 805
 Fasano, G., Poggianti, B., Bettoni, D., et al. 2003, *Mem. Soc. Astron. Italiana*, 74, 355
 Fasano, G., Vanzella, E., Dressler, A., et al. 2012, *MNRAS*, 420, 926
 Fasano, G. & Vio, R. 1991, *MNRAS*, 249, 629
 Franceschini, A., Silva, L., Fasano, G., et al. 1998, *ApJ*, 506, 600
 Fritz, J., Poggianti, B. M., Cava, A., et al. 2014, *ArXiv e-prints*
 Fritz, J., Poggianti, B. M., Cava, A., et al. 2011, *A&A*, 526, 45
 Haussler, B., McIntosh, D., Barden, M., Bell, E., & Rix, H. 2007, *ApJS*, 172, 633
 Kormendy, J. 1977, *ApJ*, 218, 333
 Liske, J., Lemon, D., Driver, S., Cross, N., & Couch, W. 2003, *MNRAS*, 344, 307
 Lotz, J. M., Madau, P., Giavalisco, M., Primack, J., & Ferguson, H. C. 2006, *ApJ*, 636, 592
 Metropolis, N., Rosenbluth, A. W., Rosenbluth, M. N., Teller, A. H., & Teller, E. 1953, *J. Chem. Phys.*, 21, 1087
 Moretti, A., Poggianti, B. M., Fasano, G., et al. 2014, *A&A*, 564, A138
 Omizzolo, A., Fasano, G., Reverte Paya, D., et al. 2014, *A&A*, 561, A111
 Peng, C., Ho, L., Impey, C., & Rix, H. 2002, *AJ*, 124, 266
 Pignatelli, E., Fasano, G., & Cassata, P. 2006, *A&A*, 446, 373
 Poggianti, B. M., Calvi, R., Bindoni, D., et al. 2013a, *ApJ*, 762, 77
 Poggianti, B. M., Calvi, R., Bindoni, D., et al. 2013b, in *IAU Symposium*, Vol. 295, *IAU Symposium*, ed. D. Thomas, A. Pasquali, & I. Ferreras, 151–154
 Poggianti, B. M., Fasano, G., Bettoni, D., et al. 2009, *ApJ*, 697, L137
 Poggianti, B. M., Moretti, A., Calvi, R., et al. 2013c, *ApJ*, 777, 125
 Saha, P. & Williams, T. B. 1994, *AJ*, 107, 1295
 Simard, L. 1998, in *Astronomical Society of the Pacific Conference Series*, Vol. 145, *Astronomical Data Analysis Software and Systems VII*, ed. R. Albrecht, R. N. Hook, & H. A. Bushouse, 108
 Simard, L., Trevor Mendel, J., Patton, D., Ellison, S., & McConnachie, A. 2011, *ApJS*, 196, 11
 Smail, I., Dressler, A., Couch, W. J., et al. 1997, *ApJS*, 110, 213
 Valentinuzzi, T., Fritz, J., Poggianti, B. M., et al. 2010a, *ApJ*, 712, 226
 Valentinuzzi, T., Poggianti, B. M., Saglia, R. P., et al. 2010b, *ApJ*, 721, L19
 Valentinuzzi, T., Woods, D., Fasano, G., et al. 2009, *A&A*, 501, 851
 Varela, J., D’Onofrio, M., Marmo, C., et al. 2009, *A&A*, 497, 667
 Vulcani, B., Poggianti, B. M., Aragón-Salamanca, A., et al. 2011a, *MNRAS*, 412, 246
 Vulcani, B., Poggianti, B. M., Dressler, A., et al. 2011b, *MNRAS*, 413, 921
 Vulcani, B., Poggianti, B. M., Fasano, G., et al. 2012, *MNRAS*, 420, 1481

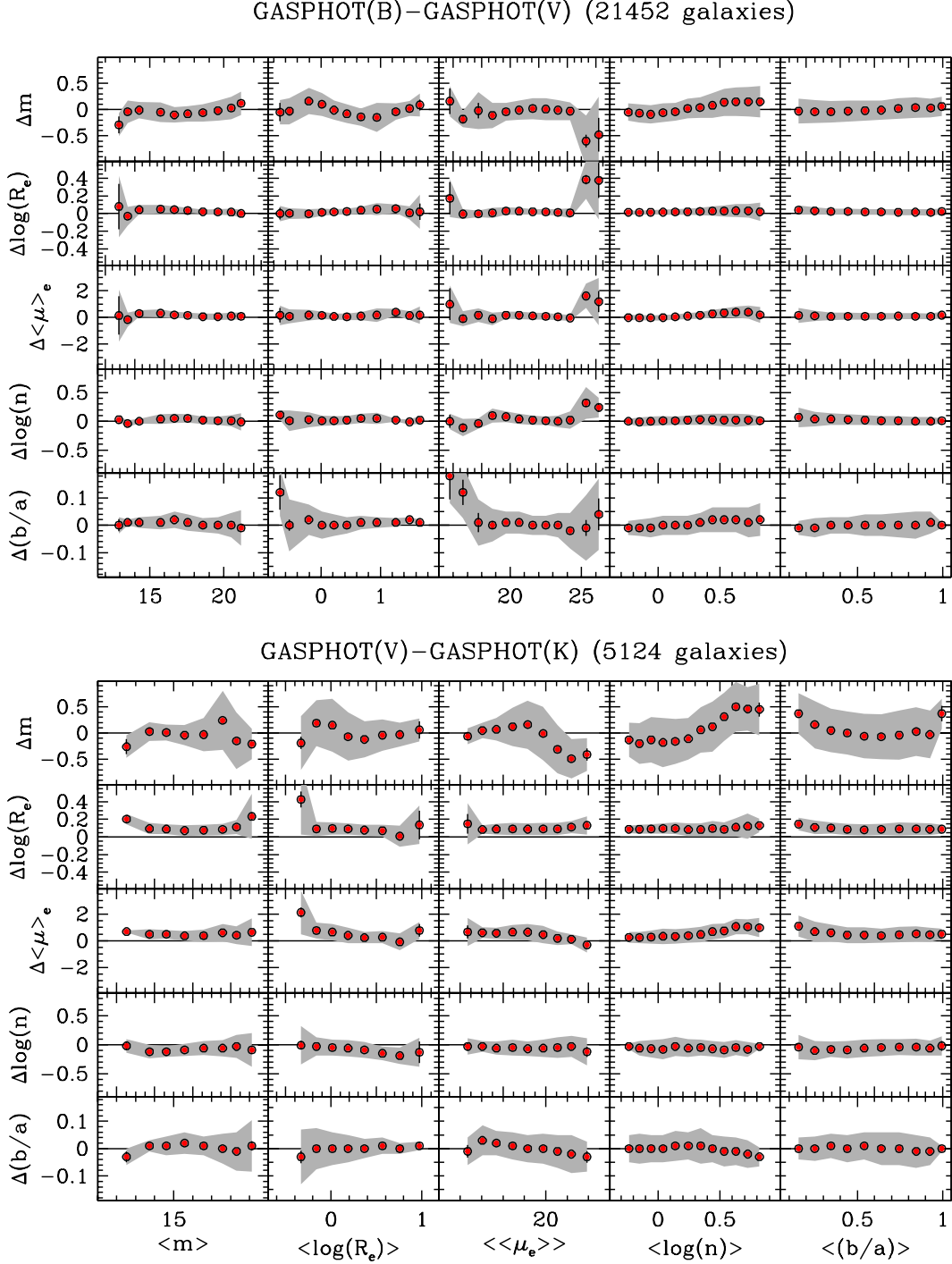


Fig. 6. Comparison among various structural parameters obtained by GASPHOT in the different bands. The upper panels refer to the B- vs. V-band comparison, while the lower panels illustrate the V- vs. K-band comparison. The differences between parameters in different bands are plotted vs. the parameters themselves, averaged between the filters under comparison. The Δm and $\Delta \langle \mu \rangle_e$ differences are ‘normalized’ by removal of the average colors (see text). As in the previous figures, the error bars represent the uncertainties of the median values of the differences in each bin, while the shaded bands give the semi-inter quartile ranges of the distributions of the deviations.

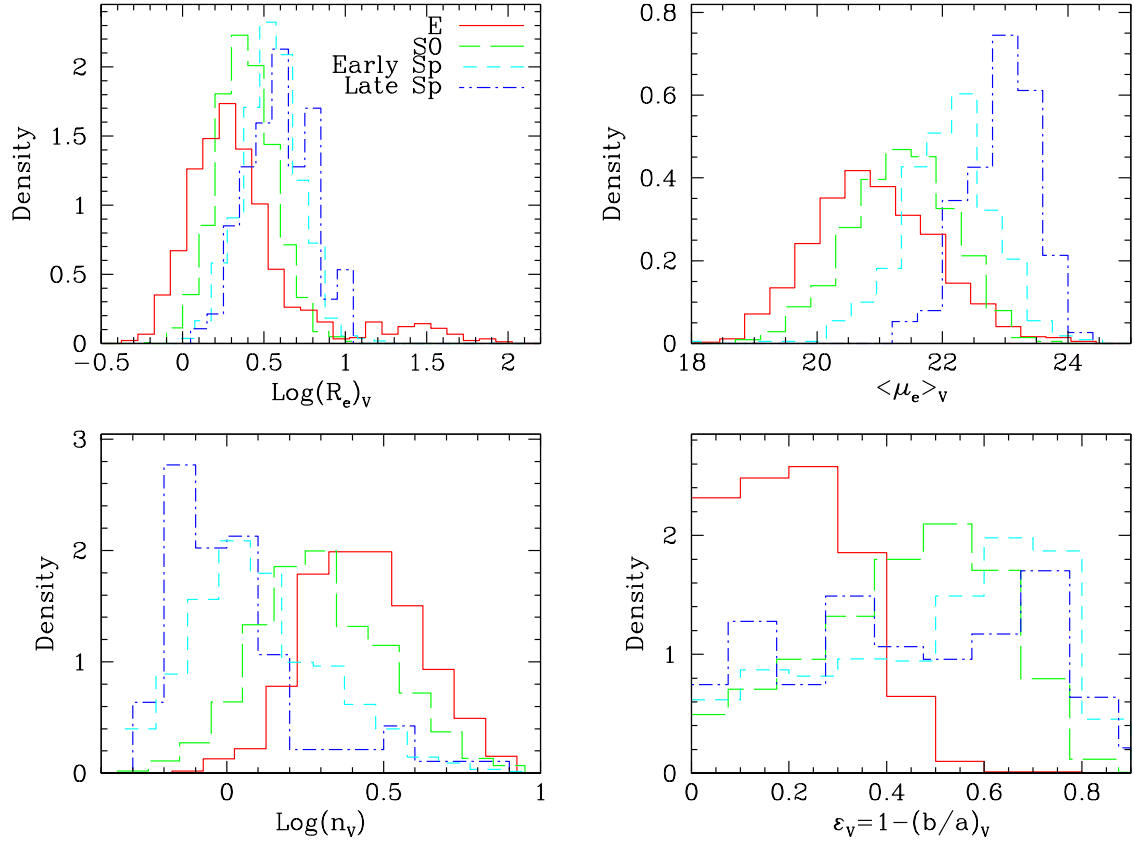


Fig. 8. Distribution of the V-band structural parameters derived by GASPHOT for the four, broad morphological types. The distributions are normalized to the area subtended by the histograms. Ellipticals, S0s, early and late spirals are respectively indicated by solid, long-dashed, short-dashed and dot-dashed lines (red, green, cyan and blue in the electronic version).

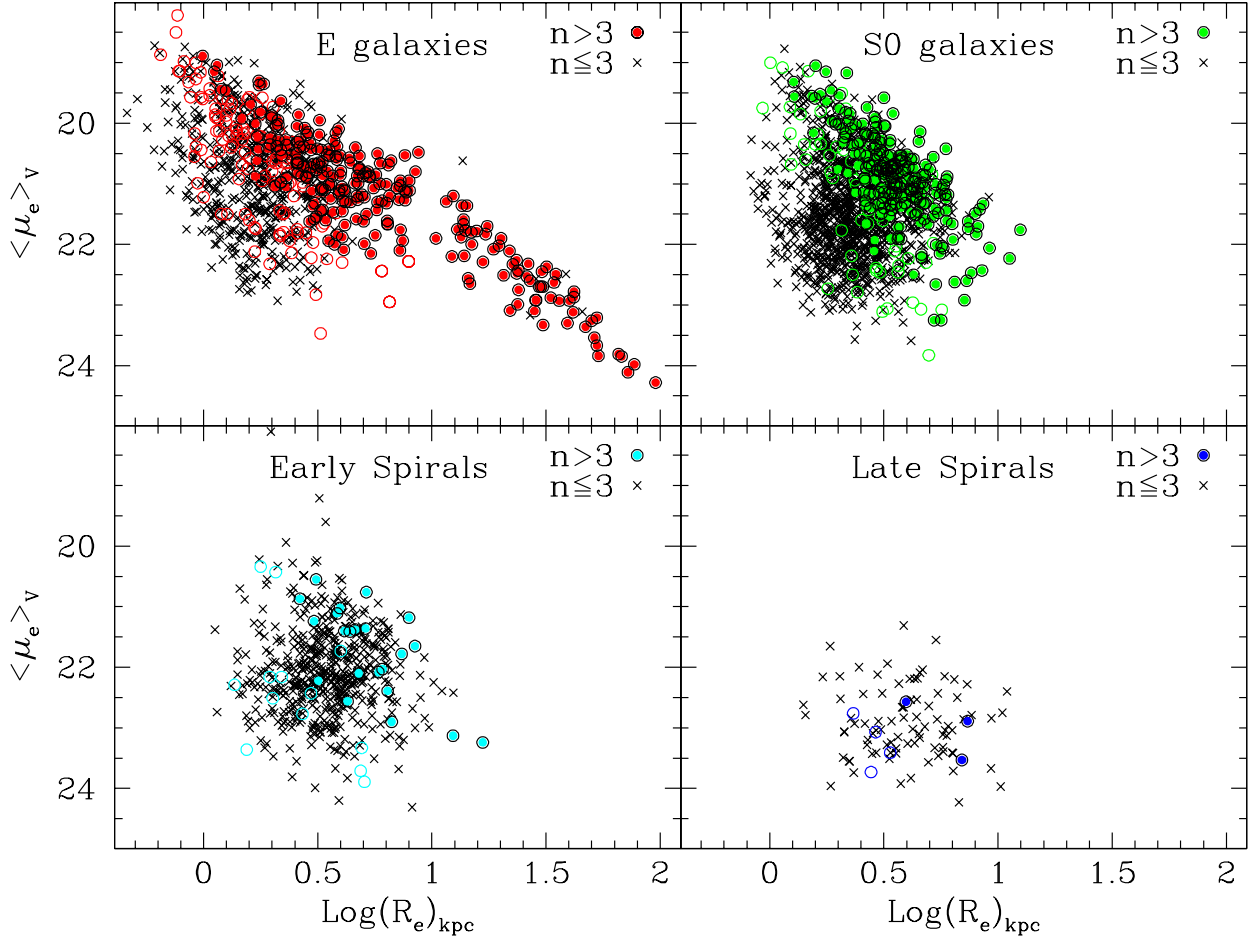


Fig. 9. The plane $\langle \mu_e \rangle - \log(R_e)$ for the galaxies of the four, broad morphological types and for two ranges of Sersic index (circles: $n > 3$; crosses: $n \leq 3$). Open circles mark galaxies with $n > 3$ and isophotal area smaller than 10^3 pixels at $2.5\sigma_{\text{bkg}}$